

# MotilA – A Python pipeline for the analysis of microglial fine process motility in 3D time-lapse multiphoton microscopy data

Fabrizio Musacchio<sup>1</sup> , Sophie Crux<sup>1</sup>, Felix Nebeling<sup>1</sup>, Nala Gockel<sup>1</sup>, Falko Fuhrmann<sup>1</sup>, and Martin Fuhrmann<sup>1</sup> 

<sup>1</sup> German Center for Neurodegenerative Diseases (DZNE), Bonn, Germany  Corresponding author

DOI: [10.xxxxxx/draft](https://doi.org/10.xxxxxx/draft)

## Software

- [Review](#) 
- [Repository](#) 
- [Archive](#) 

Editor: [Open Journals](#) 

## Reviewers:

- [@openjournals](#)

Submitted: 01 January 1970

Published: unpublished

## License

Authors of papers retain copyright and release the work under a Creative Commons Attribution 4.0 International License ([CC BY 4.0](#)).

## Summary

*MotilA* is a Python-based image analysis pipeline for quantifying fine process motility of microglia from 3D time-lapse two-channel fluorescence microscopy data. Developed for high-resolution multiphoton *in vivo* imaging datasets, *MotilA* enables both single-file and batch processing across multiple experimental conditions. It performs image preprocessing, segmentation, and motility quantification over time, using a pixel-based change detection strategy that yields biologically interpretable metrics such as the turnover rate (TOR) of microglial fine processes. While originally designed for microglial imaging, the pipeline can be extended to other cell types and imaging applications that require analysis of dynamic morphological changes. *MotilA* is openly available, platform-independent, and includes extensive documentation, tutorials, and example data to facilitate adoption by the broader scientific community. It is released under the GPL-3.0 open-source license.

## Statement of need

Microglia are innate immune cells of the central nervous system and exhibit highly dynamic, motile processes that continuously scan their environment (M. Fuhrmann et al., 2010; Nebeling et al., 2023; Nimmerjahn et al., 2005; Prinz et al., 2019; Tremblay et al., 2010). Quantifying microglial motility at the level of fine processes is crucial for studying their function in health and disease, including neurodegeneration, inflammation, and synaptic remodeling. However, despite the biological importance of this analysis, there is currently no dedicated open-source tool tailored for this task.

To date, researchers typically quantify microglial motility manually (see., e.g., Nebeling et al. (2023)) using general-purpose image processing software such as Fiji/ImageJ (Schindelin et al., 2012) or ZEISS ZEN (Carl Zeiss Microscopy GmbH, Accessed 2025). While these approaches are well established in the field, they are time-consuming, lack reproducibility, and are not well suited for batch processing or cohort-level comparisons. They often focus on individual microglia, whereas *MotilA* enables analysis of the full field of view, allowing for more comprehensive and scalable quantification. Manual workflows are also more susceptible to human bias, limiting their scalability and objectivity (Brown, 2017; Lee et al., 2024; Misra et al., 2015; Wall et al., 2018).

*MotilA* addresses these limitations by providing an end-to-end, user-friendly, and batch-capable pipeline specifically designed for 3D time-lapse two-channel microscopy data. It supports standardized workflows for single- and multi-channel datasets, integrates essential preprocessing steps (registration, spectral unmixing, histogram normalization), and derives biologically meaningful motility metrics from binarized pixel dynamics. The method builds on

strategies used in prior studies but automates the workflow in a reproducible, scalable, and open-source manner. *MotilA* thus fills a critical gap in neuroimaging analysis pipelines and is particularly valuable for labs working with multiphoton *in vivo* imaging.

## What does *MotilA* do?

*MotilA* is a modular and customizable image analysis pipeline written in Python that quantifies microglial fine process motility from time-lapse fluorescence microscopy data, typically acquired with two-photon (Denk et al., 1990; Helmchen & Denk, 2005) or three-photon *in vivo* imaging (F. Fuhrmann et al., 2024; Horton et al., 2013). Although it was originally developed for microglial analysis, the pipeline is adaptable to other cell types and imaging contexts involving dynamic morphological changes over time.

At its core, *MotilA* extracts sub-volumes from 3D time-stacks, performs 2D maximum intensity projections, and segments the resulting images to classify pixel-wise changes in microglial morphology. These changes are quantified frame-by-frame and used to calculate biologically interpretable metrics, including the turnover rate (TOR). The design is tailored to biological imaging data, with particular attention to typical issues such as z-axis projection loss, channel bleed-through, motion artifacts, photobleaching, and signal heterogeneity.

The pipeline supports both single-file processing and large-scale batch analysis. Parameters are highly customizable either programmatically or via metadata files, and all results are automatically logged, saved, and summarized for downstream statistical analysis. The outputs include segmented image series, intermediate diagnostics (e.g. histograms, projections, brightness traces), and Excel spreadsheets with motility metrics.

To accommodate large-scale, high-resolution imaging data, *MotilA* supports memory-efficient file handling via the Zarr format (Miles et al., 2025), enabling processing of large TIFF files using memory mapping to avoid RAM overload.

*MotilA* can be run via Python scripts or Jupyter notebooks, and it includes extensive documentation, examples, and a tutorial dataset to make onboarding straightforward.

We welcome community contributions and issue reports via the GitHub repository: <https://github.com/FabrizioMusacchio/motila>.

## How is “motility” determined?

*MotilA* quantifies motility by analyzing pixel-wise changes in microglial fine processes’ morphology over time. The pipeline first extracts a sub-volume around a user-defined z-axis center from each 3D image stack and applies a 2D maximum intensity projection to reduce dimensionality. Although this sacrifices some z-axis information, it enables efficient segmentation and pixel-level tracking while maintaining biological interpretability.

At each time point  $t_i$ , the projected and binarized image  $B(t_i)$  is compared to the next time point  $B(t_{i+1})$ . A temporal variation map  $\Delta B(t_i)$  is computed as:

$$\Delta B(t_i) = 2 \times B(t_i) - B(t_{i+1})$$

Based on this difference image, each pixel is classified as:

- **Stable (S)** if  $\Delta B = 1$
- **Gained (G)** if  $\Delta B = -1$
- **Lost (L)** if  $\Delta B = 2$

From these categories, *MotilA* calculates the microglial **fine process turnover rate (TOR)**, a central metric representing the fraction of pixels that changed:

$$TOR = \frac{G + L}{S + G + L}$$

This approach allows for a quantitative assessment of microglial process dynamics at each time point and across the full recording session. The same principle can be extended to other motile cell types or dynamic cellular structures where morphological changes manifest as gain or loss of segmented pixels over time.

The implementation is based on analytical strategies described in previous studies such as M. Fuhrmann et al. (2010) and Nebeling et al. (2023), with added flexibility for batch processing, filtering, and parameter tuning.

## Key features

*MotilA* offers a combination of modularity, reproducibility, and scalability specifically tailored to motility analysis in multiphoton *in vivo* imaging. Its key features include:

- **Automated preprocessing pipeline**  
Includes optional steps for image registration (2D and 3D), spectral unmixing, histogram equalization for contrast enhancement within time points, and histogram matching for brightness normalization across time points (e.g. to correct for photobleaching), as well as noise reduction via median and Gaussian filtering.
- **Flexible segmentation and thresholding**  
Supports multiple adaptive thresholding methods (e.g. Otsu, Li, Triangle) and customizable blob detection settings to isolate fine microglial processes or similar structures.
- **Pixel-based motility quantification**  
Tracks pixel-wise changes between time points to classify stable, gained, and lost pixels, allowing biologically interpretable metrics like the turnover rate (TOR).
- **Batch processing capabilities**  
Enables large-scale processing of multiple datasets with a standardized folder structure and parameter metadata sheets, suitable for cohort-level studies.
- **User-defined projection settings**  
Allows flexible extraction of sub-volumes and z-projection around multiple centers to avoid overlapping cells and vascular artifacts.
- **Memory-efficient file handling**  
Supports memory mapping of large TIFF files via the Zarr format, enabling efficient processing of high-resolution time-lapse datasets without exhausting system RAM.
- **Metadata integration and parameter logging**  
Automatically reads per-dataset settings from metadata files (e.g. Excel sheets), and stores processing parameters and outputs in structured result folders.
- **Cross-platform compatibility**  
Runs on Windows, macOS, and Linux, tested with Python 3.9 and compatible with common scientific computing environments via Conda.
- **Tutorials and example data included**  
Comes with Jupyter notebooks, example datasets, and clear documentation to help new users get started quickly.

## Pipeline steps

The *MotilA* pipeline follows a modular sequence of image processing and analysis steps designed for robust and reproducible quantification of motility from multi-dimensional imaging data. It supports both single-file and batch workflows and includes options for fine-grained customization at each step.

## 127 Core pipeline steps

128 For single datasets, *MotilA* executes the following sequence (Figure 1a)):

- 129 1. **Load image data**  
130 Supports TIFF files (Gohlke, 2025) in TZCYX (multi-channel) or TZYX (single-channel)  
131 format, following ImageJ/Fiji conventions (T: time, Z: z-axis, C: channel, Y: height, X:  
132 width).
- 133 2. **Extract sub-volumes**  
134 Selects a z-stack around a projection center for each time point, allowing focused analysis  
135 and optional multiple projections per stack.
- 136 3. **(Optional) Register sub-volumes**  
137 Applies 3D motion correction (Anuta, 1970; Guizar-Sicairos et al., 2008; Kuglin &  
138 Hines, 1975) to each time series stack using user-defined template strategies (e.g. mean,  
139 median).
- 140 4. **(Optional) Perform spectral unmixing**  
141 Removes signal bleed-through between channels, especially relevant for two-channel  
142 imaging setups.
- 143 5. **Z-projection**  
144 Projects each 3D sub-volume into a 2D image via maximum intensity projection to  
145 simplify segmentation and speed up processing.
- 146 6. **(Optional) Register projections**  
147 Aligns the 2D projections across time to correct for lateral motion artifacts.
- 148 7. **(Optional) Apply histogram equalization**  
149 Enhances local contrast within each projection using contrast-limited adaptive histogram  
150 equalization (CLAHE) (Pizer et al., 1987; Walt et al., 2014).
- 151 8. **(Optional) Apply histogram matching**  
152 Normalizes brightness across time points to mitigate bleaching effects or intensity drift  
153 (Walt et al., 2014).
- 154 9. **(Optional) Apply filtering**  
155 Reduces noise with optional median filtering (square or circular kernel) and/or Gaussian  
156 smoothing (Harris et al., 2020; Virtanen et al., 2020).
- 157 10. **Segment microglial processes**  
158 Applies adaptive thresholding (Glasbey, 1993; Li & Tam, 1998; Otsu, 1979; Prewitt &  
159 Mendelsohn, 1966; Ridler et al., 1978; Yen et al., 1995; Zack et al., 1977) and blob  
160 filtering (Fiorio & Gustedt, 1996; Walt et al., 2014; Wu et al., 2005) to identify and  
161 isolate morphologically relevant structures.
- 162 11. **Analyze motility**  
163 Quantifies pixel-level changes over time to classify stable, gained, and lost regions, from  
164 which motility metrics are derived.

165 All intermediate outputs and metrics are saved for validation and further analysis.

## 166 Batch processing steps

167 *MotilA* supports fully automated batch processing using a standardized folder structure and  
168 Excel-based metadata configuration. This enables reproducible cohort-level analysis across  
169 many animals or experimental conditions.

- 170 1. **Define a project folder**  
171 Each dataset is placed in an ID-specific subdirectory, containing imaging files, metadata,  
172 and optional result directories.
- 173 2. **Run the batch process**  
174 The core pipeline is executed for each dataset using shared or per-dataset parameters  
175 defined in metadata.xls.
- 176 3. **Save results**  
177 Segmentation outputs, projections, and motility metrics are stored in structured result

178 folders for each dataset.

#### 179 4. Batch-collect metrics

180 Aggregates metrics across datasets into cohort-level Excel files for downstream statistical  
181 analysis.

182 This design enables large-scale, reproducible quantification of microglial motility with minimal  
183 manual intervention.

#### 184 Assessing results and analyzing outputs

185 *MotilA* provides rich output in the form of diagnostic plots, intermediate image files, and  
186 structured Excel tables to support both per-dataset assessment and cohort-level statistical  
187 analysis.

##### 188 Per-dataset assessment

189 For each processed image stack, *MotilA* generates:

- 190 ■ **Segmented images and overlays** showing gained, lost, and stable regions across time  
191 points.
- 192 ■ **Histogram plots** for brightness, pixel area, and thresholding diagnostics.
- 193 ■ **Motility metrics table (*motility.xlsx*)** containing:  
194 – Gained pixels (G)  
195 – Lost pixels (L)  
196 – Stable pixels (S)  
197 – turnover rate (TOR) per time point
- 198 ■ **Brightness metrics (*brightness.xlsx*)** tracking average pixel intensity over time.
- 199 ■ **Cell area metrics (*cell\_pixel\_area.xlsx*)** reporting the segmented microglial pixel area  
200 per time point.

201 These outputs help assess segmentation quality, evaluate photobleaching or signal loss, and  
202 refine preprocessing parameters as needed.

##### 203 Cohort-level batch analysis

204 During batch processing, *MotilA* can aggregate key metrics from all datasets into shared  
205 summary files, including:

- 206 ■ *all\_motility.xlsx* — All G/L/S/TOR metrics across datasets.
- 207 ■ *all\_brightness.xlsx* — Mean brightness per dataset and time point.
- 208 ■ *all\_cell\_pixel\_area.xlsx* — Segmented area per dataset and time point.
- 209 ■ *average\_motility.xlsx* — Dataset-wise average motility metrics across the full record-  
210 ing.

211 These results allow for statistical comparison of motility dynamics across experimental conditions  
212 and facilitate downstream visualization and modeling in tools like Python, R, or Excel.

213 This multi-level output strategy ensures both technical validation and biological insight, making  
214 *MotilA* suitable for both exploratory and hypothesis-driven studies.

#### 215 Main functions

216 The three main entry points for the pipeline are:

- 217 ■ *process\_stack* — Processes a single image stack, performing the full pipeline.
- 218 ■ *batch\_process\_stacks* — Executes the pipeline across multiple datasets in a project  
219 folder.
- 220 ■ *batch\_collect* — Gathers motility metrics from all datasets for cohort-level analysis.

221 Each function supports extensive parameterization via arguments or metadata files.

222 A complete overview of configurable parameters for single-file processing, batch workflows, and  
223 image enhancement is provided in the [MotiLA README](#).

## 224 Useful helper functions

225 Several additional functions assist with data preparation and quality control, including:

- 226     ▪ `tiff_axes_check_and_correct` — Automatically adjusts TIFF axis order to TZCYX/  
227       TZYX if needed.
- 228     ▪ `hello_world` — Verifies a successful import of the *MotiLA* module.
- 229     ▪ `logger_object` — Initializes logging for the current analysis session.

## 230 Applications and limitations

231 *MotiLA* was designed with a primary focus on the analysis of microglial fine process motility  
232 *in vivo*, using high-resolution 3D time-lapse two-channel fluorescence microscopy data. Its  
233 modular design and general image processing framework, however, make it applicable to a  
234 broader range of dynamic imaging contexts.

### 235 Applications

- 236     ▪ **Microglial dynamics**  
237       Quantification of process turnover during surveillance, neuroinflammation, or disease  
238       models such as neurodegeneration and injury.
- 239     ▪ **Neuronal structural plasticity**  
240       While *MotiLA* is optimized for microglial processes, its pixel-based change detection  
241       framework can in principle be adapted to analyze dynamic changes in dendrites or axons  
242       — such as growth, retraction, or remodeling — provided the structures can be reliably  
243       segmented across time.
- 244     ▪ **Two-channel *in vivo* imaging**  
245       Effective for experiments involving simultaneous imaging of microglia and neurons (e.g.,  
246       Cx3Cr1-GFP with Thy1-YFP), with spectral unmixing to reduce bleed-through from  
247       overlapping channels or fluorophores.
- 248     ▪ **Cohort-level studies**  
249       Designed to analyze and compare motility metrics across large experimental groups,  
250       enabling high-throughput, statistically robust results.
- 251     ▪ **Teaching and prototyping**  
252       The example datasets and tutorials make *MotiLA* a useful tool for training purposes or  
253       prototyping new analysis approaches.

### 254 Limitations

- 255     ▪ **Loss of z-resolution**  
256       The use of 2D maximum intensity projections simplifies processing but sacrifices z-axis  
257       information. This may lead to overlapping structures and limits spatial specificity.
- 258     ▪ **Segmentation-dependent**  
259       Accuracy depends on appropriate thresholding and image quality. Overlapping processes,  
260       blood vessels, or low signal-to-noise ratios can reduce segmentation performance.
- 261     ▪ **Limited spectral unmixing**  
262       The current unmixing approach is a simple channel subtraction. More advanced unmixing  
263       strategies may be required for some experimental setups.
- 264     ▪ **Not a general-purpose tracking tool**  
265       *MotiLA* is optimized for pixel-level process motility, not for full cell tracking or object-based  
266       morphological quantification over time.



267     ▪ **Assumes TIFF input with standardized axis order**  
268     Input images must conform to TZCYX or TZYX structure; other formats require  
269     conversion.

270   Despite these limitations, *MotilA* provides a powerful, reproducible framework for analyzing  
271   microglial motility and similar biological processes, especially in experimental setups where  
272   manual analysis would be impractical.

## 273   Real-world example

274   To demonstrate its practical utility, *MotilA* includes a fully compatible example dataset of *in*  
275   *vivo* two-photon time-lapse imaging stacks from the mouse frontal cortex (Gockel et al., 2025).  
276   These data were acquired to assess microglial fine process motility under control conditions  
277   and during complement C4 overexpression, a genetic risk factor for schizophrenia.

278   The dataset contains two 5D TIFF stacks with the following structure:

- 279     ▪ **T**: 8 time points (5-minute intervals over 35 minutes)
- 280     ▪ **C**: 2 imaging channels (Cx3cr1-GFP for microglia, tdTomato for neurons)
- 281     ▪ **Z**: ~60 optical sections (1  $\mu\text{m}$  step size)
- 282     ▪ **Y, X**:  $\sim 1200 \times 1200$  px ( $\sim 125 \times 125 \mu\text{m}^2$  field of view)

283   The files are formatted for direct use with *MotilA*, requiring no manual reorganization or  
284   preprocessing.

285   **Figure 1** summarizes the full *MotilA* workflow as applied to the example dataset. For visu-  
286   alization purposes, the original full-field dataset was cropped around a single microglial cell  
287   to reduce background clutter and allow detailed inspection of each processing step. **Panel a)**  
288   outlines the core and optional steps in the processing pipeline. **Panel b)** shows z-projections of  
289   the microglial cell at time points  $t_0$  and  $t_1$ , including raw data, contrast enhancement, and  
290   filtering prior to segmentation. **Panel c)** displays the delta image used for motility quantification  
291   and the corresponding pixel-wise classification into stable (S, blue), gained (G, green), and lost  
292   (L, red) pixels. **Panel d)** tracks the average brightness of the segmented cell relative to the  
293   first time point, which helps assess signal stability and potential bleaching. **Panel e)** presents  
294   the turnover rate (TOR) across all time points, capturing the dynamics of microglial process  
295   remodeling.

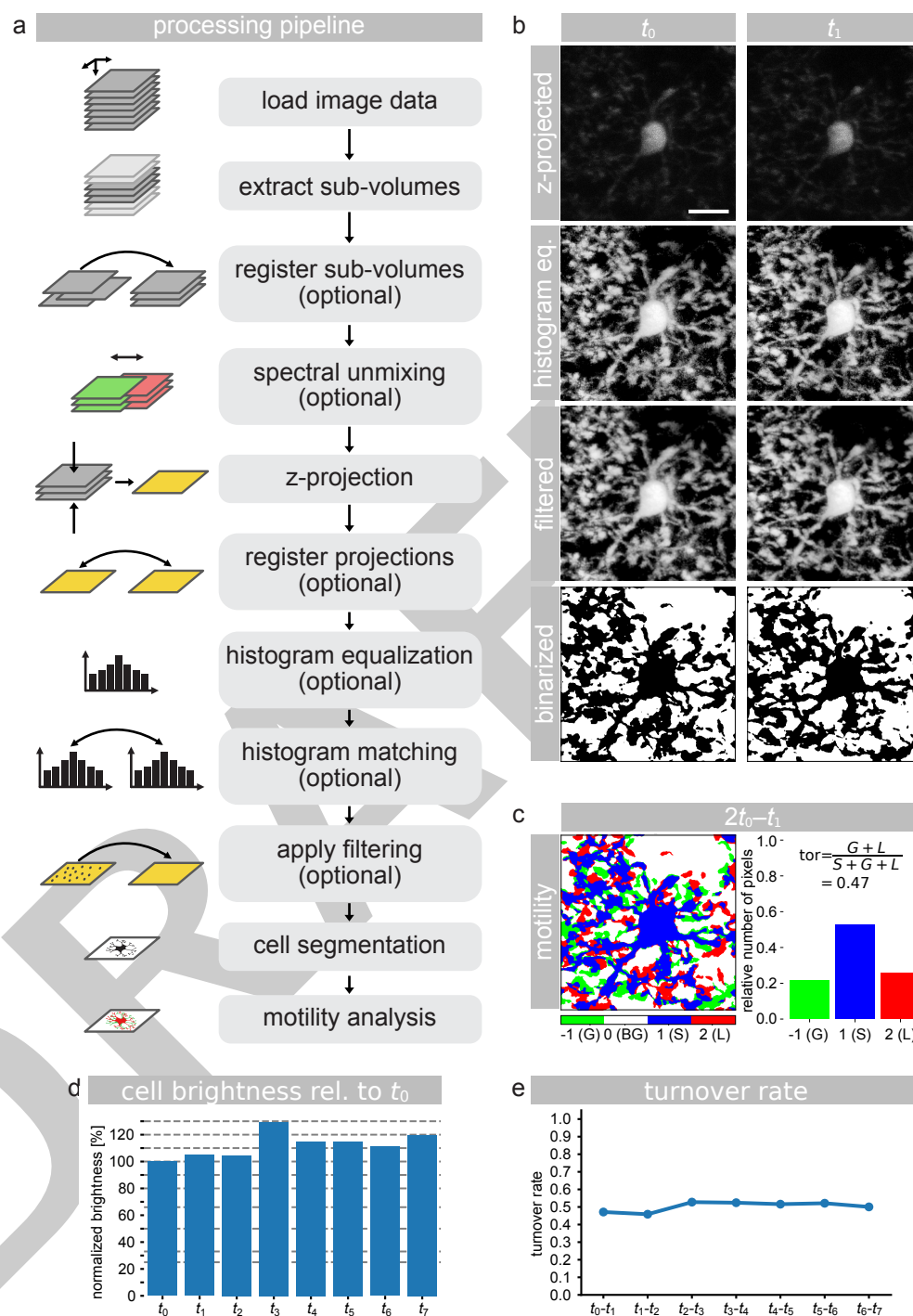


**Figure 1:** Step-by-step illustration of the *MotiLA* pipeline using the included test dataset. **a)** Overview of the image processing pipeline, showing core and optional steps. **b)** Example projections of a cropped microglial cell at time points  $t_0$  and  $t_1$ , including raw, histogram-equalized, filtered (median and Gaussian), and binarized versions. **c)** Binarized pixel-wise comparison between  $t_0$  and  $t_1$ , with classification into stable (S, blue), gained (G, green), lost (L, red), and background (BG, white) pixels, along with the corresponding pixel statistics. **d)** Normalized cell brightness over time, relative to  $t_0$ , used to assess bleaching and signal stability. **e)** Turnover rate (TOR) plotted across all time points for the same cell, representing process-level motility dynamics. All microglial image panels in **b** and **c** are shown at the same scale. Scale bar in the top-left image of panel **b** represents 10  $\mu\text{m}$ .



## Past and ongoing projects

*MotilA* has already been successfully applied in multiple neuroscience studies involving *in vivo* imaging of microglia and neurons in the mouse brain.

The following published and preprint works used *MotilA* to analyze fine process motility in physiological and pathological contexts:

- **Crux et al. (2024)**  
Investigated the role of actin depolymerizing factors ADF/Cofilin1 in microglial motility and memory formation. *MotilA* was used to quantify reduced motility in knockout mice.  
→ <https://doi.org/10.1101/2024.09.27.615114>
- **F. Fuhrmann et al. (2024)**  
Employed deep three-photon imaging of microglia in the medial prefrontal cortex to measure sub-cellular process dynamics in awake mice. *MotilA* was used to quantify microglial turnover at depths beyond 1 mm.  
→ <https://doi.org/10.1101/2024.08.28.610026>
- **Gockel et al. (2025)**  
Generated and published the example dataset accompanying this pipeline, which was used to demonstrate microglial motility changes in response to complement C4 overexpression.  
→ <https://doi.org/10.5281/zenodo.15061566>

These studies showcase the pipeline's suitability for both targeted microglial investigations and large-scale, high-resolution imaging projects. Ongoing work continues to extend *MotilA*'s application to additional brain regions, genetic perturbations, and imaging modalities, including multi-channel and high-speed two-photon datasets.

## Acknowledgements

We gratefully acknowledge the **Light Microscopy Facility (LMF)** and **Animal Research Facility (ARF)** at the German Center for Neurodegenerative Diseases (DZNE), Bonn, for their essential support in data acquisition and technical infrastructure.

This work was supported by the DZNE and by grants to MF from the European Union ERC-CoG (MicroSynCom 865618) and the German Research Foundation DFG (SFB1089 C01, B06; SPP2395). MF is a member of the DFG Excellence Cluster ImmunoSensation2. This work was also supported by the iBehave network to MF and the CANTAR (CANCerTARgeting) network to FN, both funded by the Ministry of Culture and Science of the State of North Rhine-Westphalia. The funders had no role in study design, data collection and interpretation, or the decision to submit the work for publication. FN received additional funding from the Mildred-Scheel School of Oncology Cologne-Bonn.

All animal procedures related to the example dataset were conducted in compliance with institutional, national, and international regulations. Experiments were approved by the relevant animal care and use committees at DZNE (Germany), following guidelines equivalent to the ARRIVE 2.0 framework. All efforts were made to reduce the number of animals used and to refine experimental conditions in accordance with the 3Rs (Replacement, Reduction, and Refinement) principles.

We also acknowledge the open-source community whose tools and contributions made the development of *MotilA* possible.

## References

Anuta, P. E. (1970). Spatial registration of multispectral and multitemporal digital imagery using fast fourier transform techniques. *IEEE Transactions on Geoscience Electronics*, 8(4),

- 341 353–368. <https://doi.org/10.1109/TGE.1970.271435>
- 342 Brown, D. L. (2017). Bias in image analysis and its solution: Unbiased stereology. *Journal of*  
343 *Toxicologic Pathology*, 30(3), 183–191. <https://doi.org/10.1293/tox.2017-0013>
- 344 Carl Zeiss Microscopy GmbH. (Accessed 2025). *ZEISS ZEN Microscopy Software*. <https://www.zeiss.com/metrology/en/software/zeiss-zen-core.html>.  
345
- 346 Crux, S., Roggan, M. D., Poll, S., Nebeling, F. C., Schiweck, J., Mittag, M., Musacchio, F.,  
347 Steffen, J., Wolff, K. M., Baral, A., Witke, W., Gurniak, C., Bradke, F., & Fuhrmann,  
348 M. (2024). Deficiency of actin depolymerizing factors ADF/Cfl1 in microglia decreases  
349 motility and impairs memory. *bioRxiv*. <https://doi.org/10.1101/2024.09.27.615114>
- 350 Denk, W., Strickler, J. H., & Webb, W. W. (1990). Two-photon laser scanning fluorescence  
351 microscopy. *Science*, 248(4951), 73–76. <https://doi.org/10.1126/science.2321027>
- 352 Fiorio, C., & Gustedt, J. (1996). Two linear time union-find strategies for image processing.  
353 *Theoretical Computer Science*, 154, 165–181. [https://doi.org/10.1016/0304-3975\(94\)](https://doi.org/10.1016/0304-3975(94)00262-2)  
354 [00262-2](https://doi.org/10.1016/0304-3975(94)00262-2)
- 355 Fuhrmann, F., Nebeling, F. C., Musacchio, F., Mittag, M., Poll, S., Müller, M., Giovannetti, E.  
356 A., Maibach, M., Schaffran, B., Burnside, E., Chan, I. C. W., Lagurin, A. S., Reichenbach,  
357 N., Kaushalya, S., Fried, H., Linden, S., Petzold, G. C., Tavosanis, G., Bradke, F., &  
358 Fuhrmann, M. (2024). Three-photon in vivo imaging of neurons and glia in the medial  
359 prefrontal cortex with sub-cellular resolution. *bioRxiv*. [https://doi.org/10.1101/2024.08.](https://doi.org/10.1101/2024.08.28.610026)  
360 [28.610026](https://doi.org/10.1101/2024.08.28.610026)
- 361 Fuhrmann, M., Bittner, T., Jung, C. K. E., Burgold, S., Page, R. M., Mitteregger, G., Haass,  
362 C., LaFerla, F. M., Kretschmar, H., & Herms, J. (2010). Microglial Cx3cr1 knockout  
363 prevents neuron loss in a mouse model of alzheimer's disease. *Nature Neuroscience*, 13(4),  
364 411–413. <https://doi.org/10.1038/nn.2511>
- 365 Glasbey, C. A. (1993). An analysis of histogram-based thresholding algorithms. *CVGIP:*  
366 *Graphical Models and Image Processing*, 55(6), 532–537. [https://doi.org/10.1006/cgip.](https://doi.org/10.1006/cgip.1993.1040)  
367 [1993.1040](https://doi.org/10.1006/cgip.1993.1040)
- 368 Gockel, N., Nieves-Rivera, N., Druart, M., Jaako, K., Fuhrmann, F., Rožkalne, R., Musacchio,  
369 F., Poll, S., Jansone, B., Fuhrmann, M., & Magueresse, C. L. (2025). *Example datasets for*  
370 *microglial motility analysis using the MotiLA pipeline*. Zenodo. [https://doi.org/10.5281/](https://doi.org/10.5281/zenodo.15061566)  
371 [zenodo.15061566](https://doi.org/10.5281/zenodo.15061566)
- 372 Gohlke, C. (2025). *TiffFile: Read and write image data from and to TIFF files* (Version  
373 2025.3.13). Zenodo. <https://doi.org/10.5281/zenodo.6795860>
- 374 Guizar-Sicairos, M., Thurman, S. T., & Fienup, J. R. (2008). Efficient subpixel image  
375 registration algorithms. *Opt. Lett.*, 33(2), 156–158. [https://doi.org/10.1364/OL.33.](https://doi.org/10.1364/OL.33.000156)  
376 [000156](https://doi.org/10.1364/OL.33.000156)
- 377 Harris, C. R., Millman, K. J., Walt, S. J. van der, Gommers, R., Virtanen, P., Cournapeau, D.,  
378 Wieser, E., Taylor, J., Berg, S., Smith, N. J., Kern, R., Picus, M., Hoyer, S., Kerkwijk,  
379 M. H. van, Brett, M., Haldane, A., Río, J. F. del, Wiebe, M., Peterson, P., ... Oliphant,  
380 T. E. (2020). Array programming with NumPy. *Nature*, 585(7825), 357–362. <https://doi.org/10.1038/s41586-020-2649-2>  
381
- 382 Helmchen, F., & Denk, W. (2005). Deep tissue two-photon microscopy. *Nature Methods*,  
383 2(12), 932–940. <https://doi.org/10.1038/nmeth818>
- 384 Horton, N. G., Wang, K., Kobat, D., Clark, C. G., Wise, F. W., Schaffer, C. B., & Xu, C.  
385 (2013). In vivo three-photon microscopy of subcortical structures within an intact mouse  
386 brain. *Nature Photonics*, 7(3), 205–209. <https://doi.org/10.1038/nphoton.2012.336>
- 387 Kuglin, C. D., & Hines, D. C. (1975). The phase correlation image alignment method.

- 388 *Proceedings of the IEEE International Conference on Cybernetics and Society*, 163–165.
- 389 Lee, R. M., Eisenman, L. R., Khuon, S., Aaron, J. S., & Chew, T.-L. (2024). Believing is  
390 seeing – the deceptive influence of bias in quantitative microscopy. *Journal of Cell Science*,  
391 137(1), jcs261567. <https://doi.org/10.1242/jcs.261567>
- 392 Li, C. H., & Tam, P. K. S. (1998). An iterative algorithm for minimum cross entropy  
393 thresholding. *Pattern Recognition Letters*, 18(8), 771–776. [https://doi.org/10.1016/](https://doi.org/10.1016/S0167-8655(98)00057-9)  
394 [S0167-8655\(98\)00057-9](https://doi.org/10.1016/S0167-8655(98)00057-9)
- 395 Miles, A., jakirkham, Hamman, J., Orfanos, D. P., Stansby, D., Bussonnier, M., Moore,  
396 J., Bennett, D., Augspurger, T., Rzepka, N., Cherian, D., Verma, S., Bourbeau, J.,  
397 Fulton, A., Abernathey, R., Lee, G., Spitz, H., Kristensen, M. R. B., Jones, M., &  
398 Schut, V. (2025). *Zarr-developers/zarr-python: v3.0.6* (Version v3.0.6). Zenodo. [https://](https://doi.org/10.5281/zenodo.3773449)  
399 [doi.org/10.5281/zenodo.3773449](https://doi.org/10.5281/zenodo.3773449)
- 400 Misra, I., Zitnick, C. L., Mitchell, M., & Girshick, R. B. (2015). Seeing through the human  
401 reporting bias: Visual classifiers from noisy human-centric labels. *2016 IEEE Conference*  
402 *on Computer Vision and Pattern Recognition (CVPR)*, 2930–2939. [https://doi.org/10.](https://doi.org/10.1109/cvpr.2016.320)  
403 [1109/cvpr.2016.320](https://doi.org/10.1109/cvpr.2016.320)
- 404 Nebeling, F. C., Poll, S., Justus, L. C., Steffen, J., Keppler, K., Mittag, M., & Fuhrmann,  
405 M. (2023). Microglial motility is modulated by neuronal activity and correlates with  
406 dendritic spine plasticity in the hippocampus of awake mice. *eLife*, 12, e83176. [https://](https://doi.org/10.7554/eLife.83176)  
407 [doi.org/10.7554/eLife.83176](https://doi.org/10.7554/eLife.83176)
- 408 Nimmerjahn, A., Kirchhoff, F., & Helmchen, F. (2005). Resting microglial cells are highly  
409 dynamic surveillants of brain parenchyma in vivo. *Science*, 308(5726), 1314–1318. [https://](https://doi.org/10.1126/science.1110647)  
410 [doi.org/10.1126/science.1110647](https://doi.org/10.1126/science.1110647)
- 411 Otsu, N. (1979). A threshold selection method from gray-level histograms. *IEEE Transactions*  
412 *on Systems, Man, and Cybernetics*, 9(1), 62–66. [https://doi.org/10.1109/TSMC.1979.](https://doi.org/10.1109/TSMC.1979.4310076)  
413 [4310076](https://doi.org/10.1109/TSMC.1979.4310076)
- 414 Pizer, S. M., Amburn, E. P., Austin, J. D., Cromartie, R., Geselowitz, A., Greer, T., Haar  
415 Romeny, B. ter, Zimmerman, J. B., & Zuiderveld, K. (1987). Adaptive histogram equaliza-  
416 tion and its variations. *Computer Vision, Graphics, and Image Processing*, 39(3), 355–368.  
417 [https://doi.org/10.1016/S0734-189X\(87\)80186-X](https://doi.org/10.1016/S0734-189X(87)80186-X)
- 418 Prewitt, J. M. S., & Mendelsohn, M. L. (1966). The analysis of cell images. *Annals of the*  
419 *New York Academy of Sciences*, 128(3), 1035–1053. [https://doi.org/10.1111/j.1749-6632.](https://doi.org/10.1111/j.1749-6632.1965.tb11715.x)  
420 [1965.tb11715.x](https://doi.org/10.1111/j.1749-6632.1965.tb11715.x)
- 421 Prinz, M., Jung, S., & Priller, J. (2019). Microglia biology: One century of evolving concepts.  
422 *Cell*, 179(2), 292–311. <https://doi.org/10.1016/j.cell.2019.08.053>
- 423 Ridler, T. W., Calvard, S., & name, F. (1978). Picture thresholding using an iterative  
424 selection method. *IEEE Transactions on Systems, Man, and Cybernetics*, 8(8), 630–632.  
425 <https://doi.org/10.1109/TSMC.1978.4310039>
- 426 Schindelin, J., Arganda-Carreras, I., Frise, E., Kaynig, V., Longair, M., Pietzsch, T., Preibisch,  
427 S., Rueden, C., Saalfeld, S., Schmid, B., & others. (2012). Fiji: An open-source platform  
428 for biological-image analysis. *Nature Methods*, 9(7), 676–682. [https://doi.org/10.1038/](https://doi.org/10.1038/nmeth.2019)  
429 [nmeth.2019](https://doi.org/10.1038/nmeth.2019)
- 430 Tremblay, M.-È., Lowery, R. L., & Majewska, A. K. (2010). Microglial interactions with  
431 synapses are modulated by visual experience. *PLOS Biology*, 8(11), 1–16. [https://doi.org/](https://doi.org/10.1371/journal.pbio.1000527)  
432 [10.1371/journal.pbio.1000527](https://doi.org/10.1371/journal.pbio.1000527)
- 433 Virtanen, P., Gommers, R., Oliphant, T. E., Haberland, M., Reddy, T., Cournapeau, D.,  
434 Burovski, E., Peterson, P., Weckesser, W., Bright, J., Walt, S. J. van der, Brett, M.,  
435 Wilson, J., Millman, K. J., Mayorov, N., Nelson, A. R. J., Jones, E., Kern, R., Larson, E., ...

- Contributors, S. 1.0. (2020). SciPy 1.0: Fundamental algorithms for scientific computing in python. *Nature Methods*, 17, 261–272. <https://doi.org/10.1038/s41592-019-0686-2>
- Wall, E., Blaha, L. M., Paul, C. L., Cook, K., & Endert, A. (2018). Four perspectives on human bias in visual analytics. In G. Ellis (Ed.), *Cognitive biases in visualizations* (pp. 29–42). Springer International Publishing. [https://doi.org/10.1007/978-3-319-95831-6\\_3](https://doi.org/10.1007/978-3-319-95831-6_3)
- Walt, S. van der, Schönberger, J. L., Nunez-Iglesias, J., Boulogne, F., Warner, J. D., Yager, N., Gouillart, E., Yu, T., & contributors, the scikit-image. (2014). Scikit-image: Image processing in python. *PeerJ*, 2, e453. <https://doi.org/10.7717/peerj.453>
- Wu, K., Otoo, E., & Shoshani, A. (2005). *Optimizing connected component labeling algorithms* (Technical Report LBNL-56864). Lawrence Berkeley National Laboratory, University of California. <https://doi.org/10.1117/12.596105>
- Yen, J.-C., Chang, F.-J., & Chang, S.-J. (1995). A new criterion for automatic multilevel thresholding. *IEEE Transactions on Image Processing*, 4(3), 370–378. <https://doi.org/10.1109/83.366472>
- Zack, G. W., Rogers, W. E., & Latt, S. A. (1977). Automatic measurement of sister chromatid exchange frequency. *Journal of Histochemistry & Cytochemistry*, 25(7), 741–753. <https://doi.org/10.1177/25.7.70454>

DRAFT